Anoxic iron sulfides formation for iron removal in groundwater treatment

Holst, Tjark; Goedhart, Roos; van Loosdrecht, Mark C.M.; van Halem, Doris

DOI
10.1016/j.jwpe.2025.108234

Publication date
2025

Document Version
Final published version

Published in
Journal of Water Process Engineering

Journal of Water Process Engineering 76 (2025) 108234

Contents lists available at ScienceDirect

Journal of Water Process Engineering

journal homepage: www.elsevier.com/locate/jwpe

Anoxic iron sulfides formation for iron removal in groundwater treatment

Tjark Holst [a,b], Roos Goedhart [a,*], Mark C.M. van Loosdrecht [c], Doris van Halem [a]

[a] Water Management Department, Faculty of Civil Engineering and Geosciences, Delft University of Technology, Stevinweg 1, 2628 CN Delft, the Netherlands
[b] Lenntech B.V., Distributieweg 3, 2645 EG Delfgauw, the Netherlands
[c] Biotechnology Department, Faculty of Applied Sciences, Delft University of Technology, Van der Maasweg 9, 2629 HZ Delft, the Netherlands

ARTICLE INFO

Editor: Li Gao

Keywords:
Drinking water
Iron
Groundwater
Treatment
Mackinawite
Sulfide

ABSTRACT

Groundwater is one of the major sources for drinking water supply worldwide. Conventional iron removal via aeration-filtration produces about 72,802 t of iron sludge annually in the Netherlands alone. Iron sludge comprises low-density flocs of little to no commercial value. The current study explored a novel concept for iron removal, namely anoxic iron sulfides formation in a fixed bed continuous flow reactor. Iron sulfides usually form dense structures and offer a wider range of re-use applications. A packed bed up-flow column reactor filled with pyrite granules was fed iron and sulfide containing solutions. Produced solids were analyzed applying X-ray diffraction analysis, Raman spectroscopy, digital microscopy, scanning electron microscopy and energy dispersive X-ray spectroscopy. Rapid iron sulfides formation was observed after < 10 min. The formed minerals were partially retained by the pyrite granules. The molar ratio of removed Fe(II) to removed S(-II) equaled up to 0.76 ± 0.16 mol $Fe(II)_{rem}$/(mol $S(-II)_{rem}$). Our results show that iron sulfides formation can present an interesting alternative to iron removal via aeration-filtration due to its compact particle sizes and fast formation rates.

1. Introduction

Groundwater is one of the major sources of drinking water supply worldwide. One common groundwater constituent which needs to be removed is iron. Iron concentrations in groundwater can range from 0 to > 50 mg/L. The limit set by the World Health Organization for drinking water is 0.3 mg/L [1], because elevated iron concentrations cause taste and staining issues and clogging of pipes. Conventionally, iron is removed via aeration followed by rapid sand filters. During this process Fe(II) is oxidized to Fe(III), which precipitates as $Fe(OH)_3$. Precipitated $Fe(OH)_3$ is subsequently retained by the rapid sand filter [2].

The conventional method produces strong water binding and bulky iron flocs. The formation of vast amounts of iron sludge leads to frequent energy intensive backwashing of the filters, and high energy use for the transport of iron sludge. Other disadvantages of conventional aeration-filtration are the water consumption required for backwashing and the temporary interruption of the filter operation. About 72,802 t of iron sludge are produced annually in the Netherlands alone [3]. Iron sludge is typically of little to no commercial value and only has a few applications [4].

Precipitating Fe(II) anoxically before aeration has the potential to form a product that is denser than the iron sludge currently obtained, as previously demonstrated for the phosphate mineral vivianite [5]. The formation of valueless iron sludge and filter backwash frequencies could be reduced, and the overall amount of backwash water to be treated decreased. Sulfide might be an interesting alternative precipitant. Sulfide (S(-II)) is a groundwater-native compound known to readily precipitate Fe(II) forming a wide range of compact iron sulfides [6]. Additionally, sulfide as H_2S can participate in redox reactions, with protons acting as the oxidant reduced to H_2, and sulfide serving as the reductant [7]. One commonly found iron sulfide is pyrite (FeS_2), a dense crystal often formed in anoxic sediments [8]. Other prominent iron sulfides are greigite (Fe_3S_4), mackinawite (FeS_m) and marcasite (FeS_2) the polymorph of pyrite. FeS_m is usually the first precipitate to form in anoxic iron sulfide experiments at ambient temperatures [9].

Previous investigations into the formation of iron sulfides, such as pyrite, typically aimed to understand the fundamental formation pathways in natural systems such as marine sediments [8], to study iron sulfide scale formations in engineered systems [10,11], or to produce pyrite at high temperatures for technical applications [12]. To our knowledge, this study is the first to explore the concept of S(-II) dosing for iron removal using (i) a fixed bed continuous flow reactor, (ii) a hydraulic retention time comparable to drinking water treatment plant filters (19 min), and (iii) S(-II) dosing via a dissolved sulfide containing

* Corresponding author.
E-mail address: r.c.goedhart@tudelft.nl (R. Goedhart).

https://doi.org/10.1016/j.jwpe.2025.108234
Received 16 April 2025; Received in revised form 3 June 2025; Accepted 27 June 2025
Available online 10 July 2025

solution. There has been one previous study that explored S(-II) dosing by H_2S purging for six hours in groundwater batches, achieving iron removal efficiencies of 75–83 % [13]. In addition, iron sulfides are increasingly studied for their potential use in water treatment [14–20]. This indicates that iron removal through formation of iron sulfides may be a promising alternative to conventional oxic removal, offering multiple benefits - not only removing iron but also potentially targeting other contaminants.

2. Materials and methods

2.1. Experimental set-up

Fig. 1 shows a schematic overview of the lab-scale up-flow column reactor. The column reactor was filled with granular pyrite and fed with a sulfide and a Fe(II) containing solution which mixed just before entering the reactor. In- and effluent samples were analyzed for iron, sulfide and pH. Electrical conductivity was measured inline.

Inflatable aluminum-laminate bags (3 & 10 L, Unibrew Nederland, Netherlands) were used for storing the influent media and collecting the effluent. One in- and effluent bag was operated at a time. The second bag allowed for uninterrupted operation of the reactor during replacement. The aluminum laminate provides an oxygen barrier to keep the liquid anoxic and deflates and inflates as liquid enters or leaves, respectively. A glass cylinder (117 mL) of 40.0 cm length with a diameter of 1.9 cm was selected as reactor. It has a stainless-steel mesh at the inlet and outlet. The reactor was operated in up-flow mode. Peristaltic pumps (120 U, Watson-Marlow Fluid Technology Solutions, UK) were used to feed the system and Watson Marlow Marprene tubing was used for the pumps (902.0016.016, Watson Marlow, UK). All remaining tubing were made of polyurethane (PUN-H-6X1-SW, Festo, Germany). Experiments were performed in a fume hood.

The reactor was filled with granular pyrite (Mineraliengrosshandel Hausen GmbH, Austria) sieved for a diameter range of 1.4 to 2.8 mm. Additionally, two polished cubic pyrite granules (MIKON GmbH, Germany) were added for scanning electron microscopy analysis [14]. Pyrite was added since it is known to catalyze the formation of new pyrite crystals [10,14], can provide a surface area for pyrite crystal growth and, while other iron sulfides may also have catalytic effects, pyrite is the most stable iron sulfide mineral. The pyrite was thoroughly dried and rinsed using 0.5 M HCl and deionized water.

2.2. Operational conditions

Mohr's salt ($(NH_4)2Fe(SO_4)_2{\cdot}6H_2O$) was used as Fe(II) source, as it is reported, that Fe(II) from this salt is more resistant to oxidation compared to other Fe(II) salts [6]. $Na_2S{\cdot}9H_2O$ was utilized as sulfide source [15]. There is little chemical difference between utilizing Na_2S, NaHS or $H_2S + NaOH$, with respect to iron sulfide formation studies [6]. Sodium sulfite was utilized as oxygen scavenger (79 mg/L) and $NaHCO_3$ was dosed as a pH buffer (235 mg/L). The pH was adjusted to 6.1 ± 0.1 using HCl (Honeywell, USA). Applied chemicals were of ACS Grade or higher and if not stated differently, purchased from Merck Sigma (Germany). All media were sparged using N_2-gas until an oxygen concentration of < 0.02 mg O_2/L was reached. Subsequently, solutions were prepared in a vinyl (PVC) anoxic chamber (Coy Laboratory Products, USA). The anoxic chamber was filled with a gas mixture of 5 % hydrogen and 95 % argon gas (impurity < 200 vpm). Anoxic conditions in the chamber were secured, by an airlock, weekly regenerated palladium catalysts and continuous O_2 measurements. The humidity was kept < 70 % using silica beads (confirmed by hygrometer measurements). Experiments were performed at room temperature of approximately 21 °C.

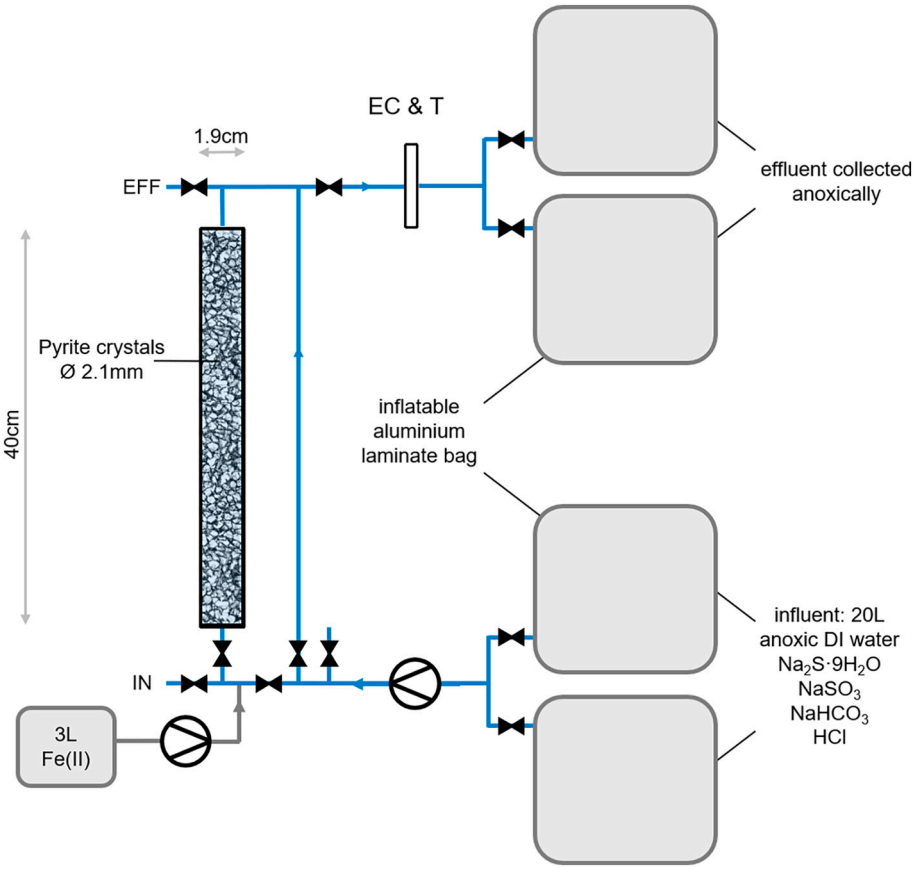

Fig. 1. Scheme of the lab-scale packed bed up-flow column reactor for iron sulfide formation. The Rectangle labelled "EC & T" represents an electrical conductivity (EC) and temperature (T) probe. In- and effluent sampling ports are indicated with "IN" and "EFF", respectively.

For the experiment the reactor was fed Fe(II) and sulfide containing solutions that mixed just before entering the reactor. Two S(-II) dosing ratios were investigated, henceforth referred to as the low and high dosing ratio. These two ratios were used to derive a relationship between dosed sulfide concentrations and respective iron removals. After dosing the high sulfide concentrations, the dose was decreased again to validate the relation between sulfide dose and iron removal. The low sulfide dosing ratio equaled 0.4 ± 0.1 mmol S(-II)/mmol Fe(II). The high dosing ratio equaled 1.1 ± 0.4 mmol S(-II)/mmol Fe(II). The incoming iron concentration was constant at 19.8 ± 1.8 mg Fe(II)/L, representing a typical level found in groundwater.

Phreeqc [16] calculations indicate the principle feasibility of iron sulfide formation at the experimental conditions. The calculated saturation indices were 2.1 and 17.3 for FeS_m and pyrite at the low dosing ratio and 2.2 and 17.5 for FeS_m and pyrite at the high dosing ratio, respectively.

Prior to starting the experiments, anoxic conditions were confirmed by dissolved oxygen measurements. The reactor inflow was adjusted to 185 mL/h leading to an average hydraulic retention time (HRT) of 19 min. The HRT was chosen to reflect typical values in drinking water treatment plant filters and because iron sulfide precipitation at the investigated concentrations typically completes within minutes [17]. The porosity used for calculating the HRT was 0.49 (57 ± 1 mL) and was estimated using a salt tracer and physical considerations (see SI 1).

2.3. Analysis of dissolved constituents

Prior to use, sampling syringes were flushed using N_2 gas. Media was drained for two minutes through the sampling port before connecting the syringe to ensure anoxic conditions. The iron concentration was quantified using Hach method LCK 320 & LCK321 (Hach Lange GmbH, Germany). The pH was estimated using a sulfide resistant probe (InPro 3250i/SG/225, Mettler Toledo, Switzerland). An optical IDS sensor (FDO® 925, Xylem Analytics, USA) was used for dissolved oxygen measurements and the electrical conductivity was measured using a TetraCon® 925 (Xylem Analytics, USA).

S(-II) concentrations were determined using the methylene blue method applying Hach tests LCK653. S(-II) samples were analyzed immediately. However, a few sulfide samples were conserved by immediate addition of zinc acetate and NaOH for later analysis [18]. They were stored in the fridge prior to analysis. Conservation stabilizes the samples for at least seven days [19]. Successful conservation was confirmed by own measurements. If not otherwise specified, all uncertainty ranges indicate the standard deviation.

2.4. Analysis of solid phases

Two kinds of solids were analyzed, namely, suspended solids in the effluent and the pyrite granules. Effluent suspended solids were analyzed applying X-ray diffraction (XRD), and Raman Spectroscopy. Pyrite granules were analyzed using a digital microscope, scanning electron microscope (SEM) and SEM-energy-dispersive X-ray spectroscopy (EDX).

2.4.1. Collection

The effluent was collected in the aluminum laminate bags. The bags were first flushed using N_2 gas and then evacuated before being connected to the system to ensure that the collected effluent remained free from oxygen. Subsequently, the effluent was filtered to collect any formed solids on a filter paper disc. A Nalgene™ Reusable Filter Unit (Thermo Fisher Scientific Inc., USA) with three openings on top was used. After placing the 0.1 μm filter paper discs (Cyclopore Track Etched Membrane, Whatman, USA) the headspace was flushed using N_2 gas for five minutes. The effluent bag was directly connected to the top part of the filter unit and the media was slowly added to the filter unit. The headspace of the filter unit was flushed using N_2 gas throughout the filtration process to keep the media anoxic. After filtration, the filter papers discs were immediately moved to the anoxic chamber where they were dried prior to analysis.

2.4.2. XRD

X-ray diffraction analysis was performed using a D8 Advance Eco (Bruker Corporation, USA) to identify any formed crystallographic structure that flushed out from the up-flow column reactor. Analysis was performed on the solids retained on the filter paper discs. XRD patterns were collected in the range of 5–90° 2θ using the following settings: 0.6 mm receiving slit, 0.1 s/0.0103° 2θ counting time.

2.4.3. Raman spectroscopy

Raman spectroscopy was carried out using a Renishaw Invia Reflex (Renishaw, UK). Solids retained on the filter paper disc were analyzed under the following settings: 515 nm, 1 % I of 50 mW, 20 acc, dwell time 2 s, center range 1050 cm^{-1}.

2.4.4. Digital microscope

A digital microscope (VHX-500, Keyence Corporation, Japan) was used to take pictures of the pyrite granules before and after the experiments. Pyrite granules were dried in an anoxic chamber containing silica desiccants.

2.4.5. SEM-EDX

Scanning electron microscopy and energy dispersive X-Ray spectroscopy were performed on two polished cubic pyrite granules to investigate whether any crystal growth, mineral depositing or surface transformation had occurred. The polished pyrite cubes were analyzed before and after the experiments. We used a NovaNano SEM (FEI, USA).

Before the experiments pyrite granules were immersed in 0.4 M HCl for ten minutes followed by polishing using a wool felt and subsequent cleaning with deionized (DI) water. After the experiments pyrite granules were taken from the reactor after draining the remaining anoxic water by flushing the column using N_2-gas. The column was then sealed and moved to the anoxic chamber to withdraw the polished cubic pyrite granules.

One face of each cubic pyrite crystal was analyzed. Half of the analyzed face was gently cleaned using a cosmetic tissue followed by rinsing with DI water. Afterwards the cubes were immediately freeze dried and Au-coated prior to analysis.

3. Results

3.1. Iron removal through sulfide dosage

A packed bed up-flow column reactor filled with pyrite granules was operated for the treatment of anoxic Fe(II) containing water (Fig. 2). The average iron influent concentration equaled 19.8 ± 1.8 mg Fe(II)/L and the average influent sulfide concentration was 5.3 ± 1.6 mg S(-II)/L and 11.3 ± 2.5 mg S(-II)/L for the low and high dosing ratio, respectively. During the low dosing ratio, the effluent Fe(II) concentration was relatively high, 18.4 ± 0.5 mg Fe(II)/L (pore volume 0–240 and 900 onwards), removing an average of 2.4 ± 0.4 mg Fe(II)/L from the water. Increasing the sulfide dose led to a 4-fold increase in Fe(II) removal, reaching an average of 9.9 ± 1.5 mg Fe(II)/L in the effluent (between 500 and 730 pore volumes). The average effluent sulfide concentration equaled 1.2 ± 0.5 mg S(-II)/L and 4.6 ± 1.6 mg S(-II)/L for the low and high sulfide dosing, respectively. Effluent sulfide includes FeS bound sulfide; the methodology does not make it possible to distinguish free and bound sulfides. Thus, it remains unclear whether the dosed sulfide had entirely reacted with the iron in the column. A comparison between filtered (0.22 μm nanopore filter) and unfiltered effluent samples indicated 55 % lower sulfide concentrations for the filtered samples. Notably, part of the sulfide oxidized in the influent bag before entering the reactor.

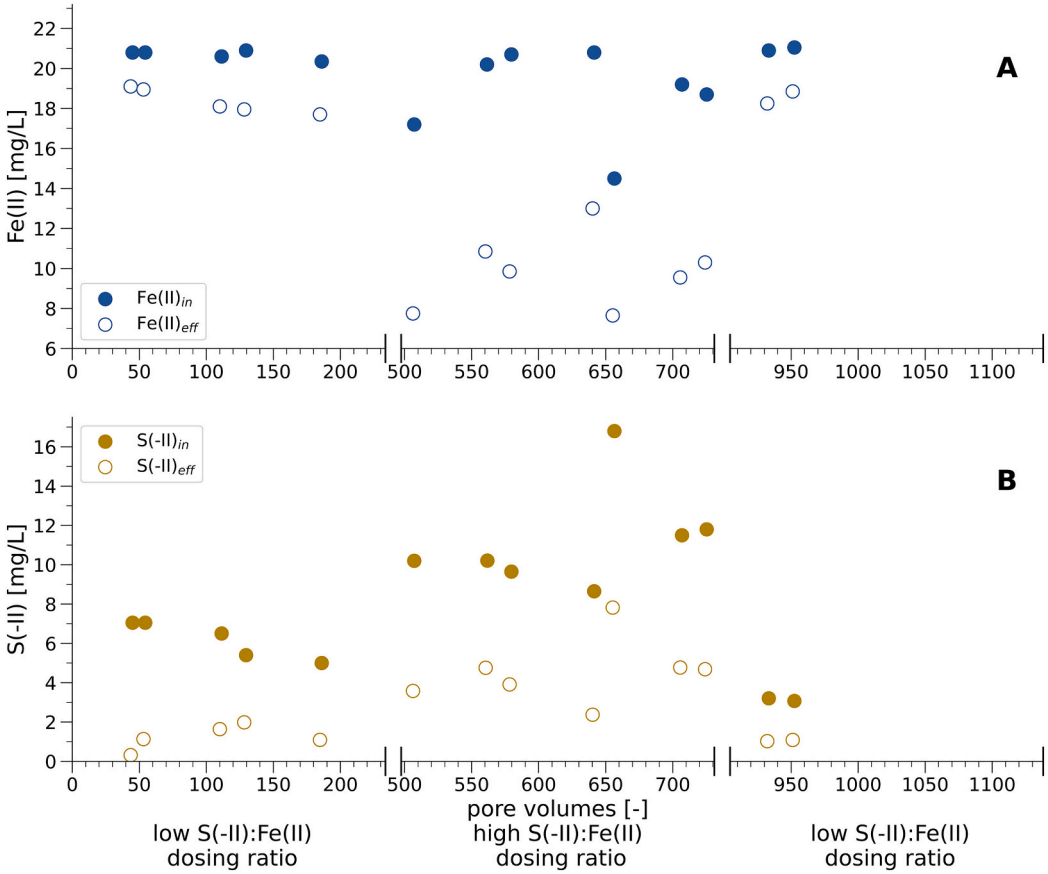

Fig. 2. Iron (A) and sulfide (B) concentrations in the influent (closed circles) and effluent (open circles) in the up-flow packed bed reactor. Experiments were conducted at a low (0–240 and 900–960 pore volumes) and high (500–730 pore volumes) sulfide concentration in the influent. HRT = 19 min.

The pH for the low Fe/S dosing ratio was 6.1 ± 0.1 for the in- and effluent. The pH for the high Fe/S dosing ratio was 6.0 and 5.9, for the in- and effluent respectively. The effluent electrical conductivity was 682 ± 19 µS/cm and 723 ± 49 µS/cm, for the low and high dosing ratio respectively.

3.2. Iron to sulfide ratio

The ratio of removed Fe(II) over removed sulfide for the low and high dosing ratio is given in Fig. 3. Higher levels of removed Fe(II) per removed sulfide were observed for the high dosing ratio. The removed Fe(II) and sulfide concentrations were calculated for each time point by subtracting the respective effluent from the influent concentration. The absolute standard deviation was approximately 0.15 for both dosing ratios. The dashed lines indicate the theoretical molar Fe:S ratios for iron sulfide minerals pyrite (0.5) and mackinawite (1.0).

3.3. Deposits on pyrite granules

Fig. 4 shows digital microscopy pictures of pristine and recovered pyrite granules after reactor operation. Clear black deposits can be seen on the pyrite granule recovered after the experiment (Fig. 4B) compared to the pristine one (Fig. 4A). The formed deposits could easily be wiped off from the pyrite granule, which is illustrated in Fig. 4C. Following a gentle cleaning, the shiny area marked with the red frame regained its pre-experiment appearance.

To examine potential occurrences of crystal growth, mineral deposition, and surface transformation, and to determine the elemental composition of the surface SEM and SEM-EDX analyses were performed. Fig. 5 shows the polished pyrite surface before and after the experiment.

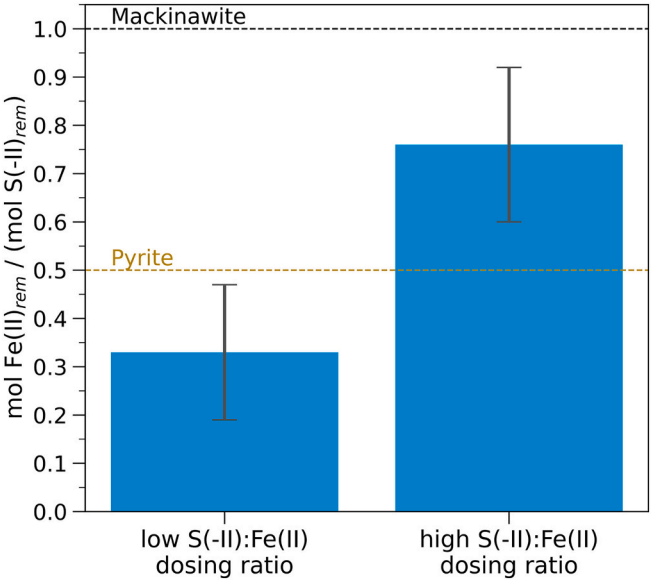

Fig. 3. Molar ratios of removed Fe(II) to removed sulfide. Error bars indicate the standard deviation. For reference, dashed lines are added indicating molar ratios of Fe:S for mackinawite (FeS_m) and pyrite (FeS_2).

SEM-EDX analysis revealed the presence of sulfur and iron minerals on the pyrite cubes. No evidence of pyrite crystal growth was found. The white leaf-like shape in the center of Fig. 5B is most likely an irregularity of the crystal itself, rather than a structure which formed during the

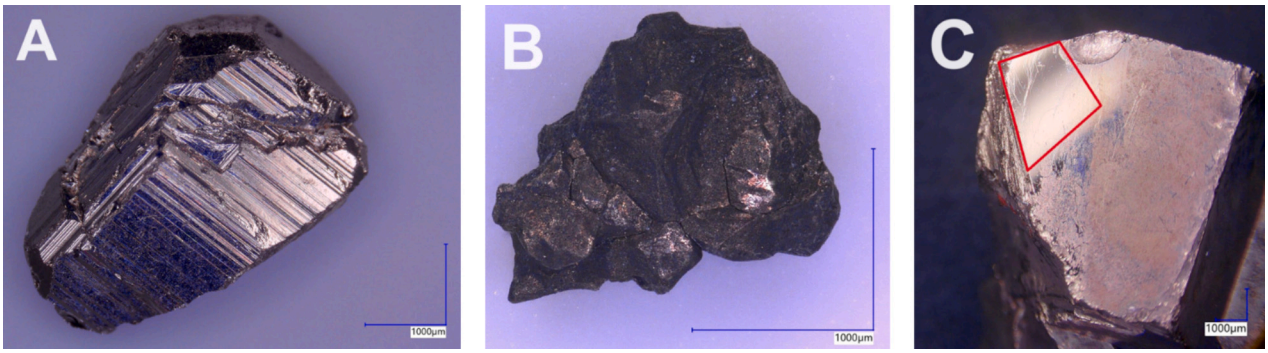

Fig. 4. Digital microscope images of pyrite granules. Pristine pyrite granule (A). Pyrite granule recovered at the end of reactor operation (B). Polished pyrite cube recovered at the end of reactor operation; a part of the surface was gently wiped off using a cosmetic tissue and rinsed with anoxic DI-water (red framed area) (C).

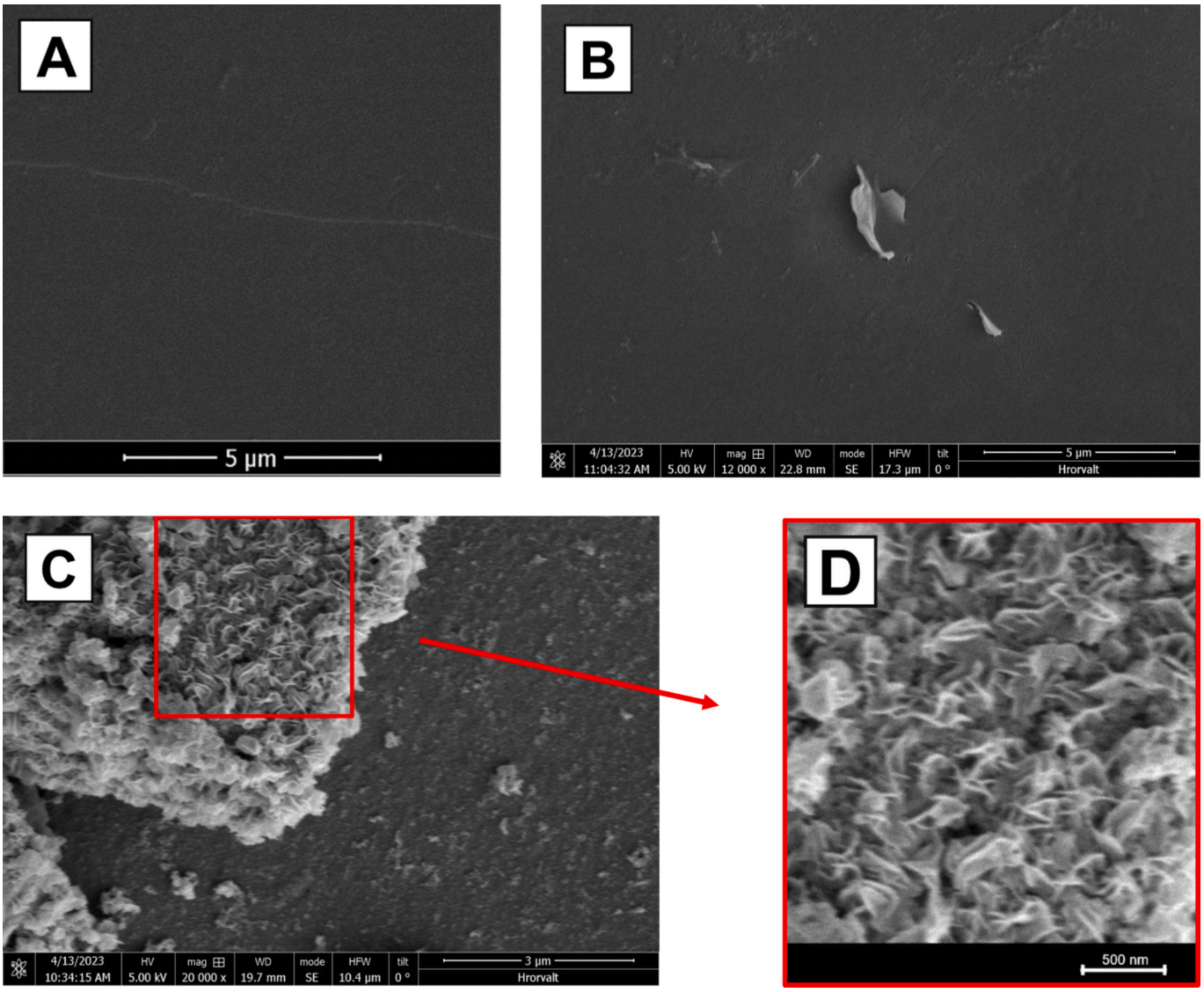

Fig. 5. SEM images of polished pyrite surface before the experiment (A). Images after the experiment of gently wiped and rinsed surface (B) and solely rinsed surface (C). D shows an amplification of C.

experiments.

The average ratio of Fe:S detected at the pyrite surface equaled 1.0:4.5 ± 0.6 (n = 4) and was estimated using SEM-EDX.

3.4. Suspended solids in water

Both influent and effluent visually contained black suspended solids (Fig. 6). Raman spectroscopy indicated the presence of rhombic sulfur (Fig. 7A and B) and pyrite (Fig. 7C) in the effluent filter residues

Fig. 6. Syringe filled with an influent sample taken during the high sulfide dosing.

collected during the high sulfide dosing [20]. Note that most analyzed samples did not result in any identifiable Raman spectra. No samples delivered an interpretable Raman spectrum for the lower sulfide dose. XRD analysis could not identify any crystalline structures on the anoxic filter residues. Oxidized filter samples indicated the presence of the iron oxyhydroxide lepidocrocite (see SI 2).

4. Discussion

4.1. Particulate iron sulfides formation

The current investigation successfully demonstrated iron removal via sulfide dosing. One possible mechanism for iron removal was the formation of mackinawite. FeS_m forms from the reaction of HS^-, H_2S or polysulfides with Fe(II), becomes visible in solutions as black discoloration and usually is nanocrystalline [21]. In this study, the sampled influent clearly showed a black discoloration (Fig. 6).

Applying the rate equation for FeS_m formation to the investigated conditions of about 19.8 mg Fe(II)/L and 11.3 mg S(-II)/L yields in initial formation rates that suggest a depletion of reactants in approximately 6.6 min [8]. This is a third of the applied HRT and matched well with the observation that most of the black precipitates retained in the bottom half of the up-flow-column reactor.

Several studies observed mackinawite formation under similar conditions. It is generally mentioned as the first precipitate to form in anoxic iron sulfide formation experiments at ambient temperatures [8,9]. Especially, in studies towards pyrite formation it has been observed [6] due to its rapid formation kinetics and low solubility [22]. In the current investigation the SEM image in Fig. 5D shows similarities to images of mackinawite [23]. Additionally, lepidocrocite, an oxidation product of FeS_m [24] was identified.

Mackinawite is difficult to detect applying XRD and Raman analysis. Firstly, the nanocrystalline FeS_m is sensitive to oxidation [6,25,26]. Even though handled carefully, it cannot be excluded that FeS_m oxidized before analysis. Secondly, the nanocrystalline size is too small to be detected by XRD [6]. XRD therefore indicates it is an amorphous state, although it is not [27]. Future investigation could utilize Mössbauer spectroscopy. Mössbauer spectroscopy seems to overcome the issue of nano crystallinity, since it does not require long-range ordering of the crystal structure [25]. The clear black discoloration of the influent samples and comparison to similar studies suggest that mackinawite was the main iron sulfide formed in this investigation. The molar ratios of removed Fe(II) to S(-II) do not equal the mackinawite ratio (1:1) (Fig. 3), suggesting that other reactions took place leading to the removed Fe(II) to S(-II) ratios.

Minor amounts of pyrite were detected in the suspended solids in the effluent. There are three mechanisms that can explain pyrite formation in this investigation. These can be categorized in nucleation and crystal growth [8]. Nucleation can occur via the polysulfide [8,28–30] and H_2S pathway [8,28,31,32], crystal growth via the congruent dissolution reaction [8]. All these pathways are thermodynamically favorable at investigated conditions [6].

In this study, pyrite formed most likely via the H_2S-paythway. H_2S and Fe(II) were present in sufficient concentrations for the SI to exceed 11 and pyrite granules were present to catalyze the reaction [8]. Pyrite formation via the polysulfide pathway is unlikely, because polysulfides only make up a minor fraction at the investigated pH of 6.0 ± 0.2 [33]. Also, the polysulfide pathway is about two magnitudes slower than the H_2S-pathway [28]. Lastly, crystal growth likely did not occur, since FeS_m would form more rapidly than pyrite [8] under the studied experimental conditions. Thus, FeS_m would have depleted the reactants for crystal growth.

4.2. Iron sulfides retention in column and competing formation pathways

It is assumed that rhombic sulfur accounts for the relatively low Fe:S ratio of 1.0:4.5 ± 0.6 on the pyrite cubes surface, measured by SEM-EDX. Therefore, also leading to the relatively low $Fe(II)_{rem}$:$S(-II)_{rem}$ ratios (Fig. 3). Note that, a ratio of 1:1 would be expected if pyrite

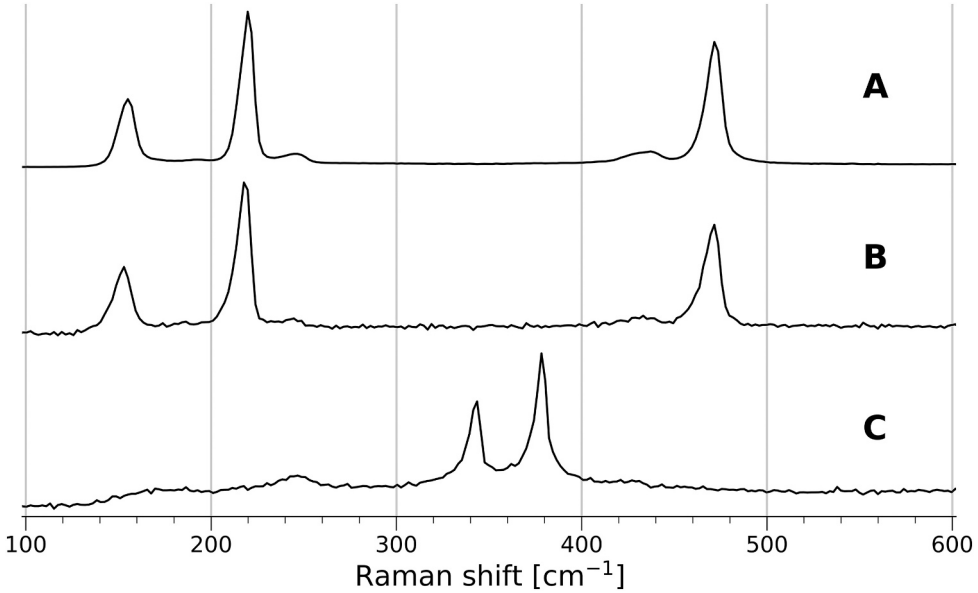

Fig. 7. Raman pattern of effluent suspended solids. A–C were retrieved from solids retained during the high sulfide dose. A and B show peaks at 152, 218 and 472 cm^{-1} indicating the presence of rhombic sulfur. C shows peaks at 342 and 378 cm^{-1} indicating the presence of pyrite.

formation does not occur and S(-II) would only be consumed by FeS_m formation. Rhombic sulfur likely formed through the oxidation of sulfide by oxygen since millimolar sulfide solutions are sensitive to oxidation [8]. Part of the sulfide appears to have oxidized to rhombic sulfur prior to entering the reactor. Moreover, Fe(III) impurities could have caused S(-II) oxidation [17] and the dosed sulfite could have oxidized part of the S(-II) leading to rhombic sulfur formation [34]. To provide direct evidence of rhombic sulfur on the pyrite granules, a follow-up study could employ X-ray photoelectron spectroscopy (XPS) or sulfur isotope analysis.

Impurities of Fe(III) and the dosed sulfite likely also contributed to the differences in removed Fe(II) to removed S(-II) ratios shown in Fig. 3. For the low and high sulfide dosing the ratios were 0.33 ± 0.14 and 0.76 ± 0.16 $Fe(II)_{rem}$:$S(-II)_{rem}$, respectively. Assuming the offset from impurities is consistent across both conditions and that FeS_m is the primary iron sulfide formed, this suggests that a greater fraction of sulfide at the low dosing level reacts with sulfite and Fe(III), leaving less available for Fe(II) removal. As a result, the removed Fe(II) to removed S(-II) ratio is lower at the lower sulfide dose. Note that the removed Fe(II) to removed S(-II) ratios in Fig. 3 do not directly represent the stoichiometry of formed solids. This is due to the consumption of sulfide by Fe(III) impurities and sulfite and because some solids might have flushed out. Moreover, the applied analytical method did not allow differentiation between bound and free sulfides in the effluent.

The pyrite granules led to the retention of iron sulfides in the reactor. This retention likely occurred through two mechanisms: (i) filtration, where particulate iron sulfide aggregated and got trapped based on size, and (ii) electrostatic interactions. The mechanism of electrostatic interaction is illustrated by comparing the point of zero charges (PZC) for the iron sulfide FeS_m and pyrite with the pH during the experiments. The PZC of FeS_m equals pH = 7.5 [21]. Meaning the FeS_m surface is charged positively at a pH < 7.5 and negatively at a pH > 7.5. The PZC of pyrite is pH 2 in the absence of potential-determining ions and pH 5 in the presence of potential-determining ions, specifically around 28 mg Fe(II)/L [35]. This implies that, at the measured pH of approximately 6.0 ± 0.1, the pyrite surface is negatively charged, while the FeS_m surface is positively charged. The opposite surface charges probably led to the retention of FeS_m on the pyrite granules surface. The pyrite granule bed did not catalyze pyrite formation nor served as a base for pyrite crystal growth, as reported elsewhere [10]. One possible explanation is that rhombic sulfur and iron sulfide deposits coated the surface of the pyrite crystals, significantly reducing the available catalytic surface area.

4.3. Prospects on iron sulfides formation for groundwater treatment

This study has shown rapid anoxic iron sulfides formation in solution upon sulfide dose and achieved a molar $Fe(II)_{rem}$:$S(-II)_{rem}$ of up to 0.76 ± 0.16 (Fig. 3). Experimentally observed iron sulfides formation characteristics indicated general applicability for typical groundwater treatment settings for two reasons. Firstly, iron sulfides formed rapidly within a timeframe of < 10 min which allows for small reactor design. Secondly, iron sulfides could be retained. The design and operational parameters need to be optimized for the formation and retention of iron sulfides. Moreover, interactions with other ions commonly found in groundwater, such as Mn^{2+} and Ca^{2+}, need to be investigated.

In a typical groundwater treatment scheme for drinking water production this technique could be placed after groundwater extraction and before aeration and filtration. Therefore, the number of backwashes is drastically reduced, while compact iron sulfides are produced instead of low-value bulky iron sludge. Formed particulate iron sulfide would need to be separated prior to aeration. A potential method to separate formed particles is filtration. Additionally, the hypothesized electrostatic removal of FeS_m particles could be further investigated. FeS_m could potentially be removed via an oppositely charged surface. For instance, an electrically charged surface, which allows for charge dependent adhesion and detachment.

In-situ electrochemical sulfate reduction producing S(-II) could provide a viable solution for iron sulfide formation. This approach would make chemical sulfide dosage redundant since groundwater native sulfate could be reduced electrochemically to S(-II) [36,37]. Fortunately, sulfate concentrations often exceed iron concentrations to such an extent that in-situ electrochemical S(-II) formation could provide sufficient reactants even for pyrite (FeS_2) formation (groundwater data in [38]). Aeration facilities can remove excess sulfide that might escape from an iron-sulfide formation reactor. It is estimated that aeration removes H_2S concentrations up to 2 ppm [39].

The estimated costs for electrochemical generation of sulfide to treat a groundwater containing 10 mg Fe(II)/L equal 0.012 €/m^3, for the formation of the iron sulfide mackinawite (see SI 3 for details). These additional costs might be balanced by the sale of produced iron sulfides, and lower transport and disposal costs. Additionally, filter backwash frequencies and backwash water treatment can be reduced. The principle feasibility of in-situ electrochemical sulfate reduction producing S(-II) has been demonstrated [36,37,40]. A previous investigation showed in-situ electrochemical generation of H_2S for a fluidized bed reactor reporting a precision of ±0.25 % in concentration ranges of 0.06 and 1900 μmol L^{-1} [40].

The rapidly formed iron sulfides do not only remove iron, but have several properties that allow to be employed for further treatment of water. For instance, FeS_m could be used for the simultaneous treatment of As(III). Although, As(III) sorps better to ferrihydrites, also FeS_m can be used as As(III) adsorbent [41]. The adsorption capacity of As(III) to FeS_m was estimated to equal 0.012 mol As(III) per mol FeS_m [42]. Converting this to Fe(II) equals a capacity of 16 μg As(III)/mg Fe(II). Next to adsorption, also formation of minerals such as orpiment (As_2S_3), realgar (AsS) and arsenopyrite (FeAsS) are proposed for arsenic immobilization [43]. Yet, it should be noted that As speciation in the presence of sulfide is complex and requires applied investigations. Other literature suggests iron sulfides have potential for co-removal of metals, organic contaminants and nutrients, such as nitrogen and phosphate [26,44,45]. More recently also removal of chromium [46], PFOA [47] and pharmaceuticals [48] are linked to iron sulfide formation, illustrating their potential wide range of interest.

5. Conclusions

This study has provided a novel perspective on anoxic groundwater treatment for drinking water production. It demonstrated the principal feasibility of iron removal via sulfide dosing in a fixed bed continuous flow reactor. We have revealed that iron sulfides formation can present an interesting alternative to conventional aerobic iron removal, due to its fast formation rates (< 10 min) and relatively compact particle sizes. The molar ratio of removed Fe(II) to removed S(-II) equaled up to 0.76 ± 0.16 mol $Fe(II)_{rem}$/(mol $S(-II)_{rem}$). Further investigations are needed to optimize the design and operational parameters for the formation and retention of iron sulfides in groundwater treatment.

CRediT authorship contribution statement

Tjark Holst: Writing – review & editing, Writing – original draft, Visualization, Validation, Resources, Methodology, Investigation, Formal analysis, Data curation, Conceptualization. **Roos Goedhart:** Writing – review & editing, Visualization, Validation, Methodology, Investigation, Formal analysis, Conceptualization. **Mark C.M. van Loosdrecht:** Writing – review & editing, Visualization, Validation, Methodology, Formal analysis, Conceptualization. **Doris van Halem:** Writing – review & editing, Visualization, Validation, Supervision, Project administration, Methodology, Investigation, Funding acquisition, Formal analysis, Conceptualization.

Declaration of competing interest

The authors declare that they have no known competing financial interests or personal relationships that could have appeared to influence the work reported in this paper.

Acknowledgements

This research is funded by NWO Dutch Research Council (Vidi grant 18369). The authors would like to thank Roald van der Kolk from the Department of Applied Sciences at the Delft University of Technology for the SEM, SEM-EDX and Raman Spectroscopy analysis. Furthermore, we would like to thank Xiaohui Liu for the XRD analyses. In addition, we extend our gratitude to Nadia van Pelt for proofreading of this manuscript.

Appendix A. Supplementary data

Supplementary data to this article can be found online at https://doi.org/10.1016/j.jwpe.2025.108234.

Data availability

Data will be made available on request.

References

[1] World Health Organization, Guidelines for drinking-water quality. https://apps.who.int/iris/handle/10665/44584, 2011. (Accessed 31 January 2023).
[2] C.G.E.M. Van Beek, J. Dusseldorp, K. Joris, K. Huysman, H. Leijssen, F. Schoonenberg Kegel, W.W.J.M. De Vet, S. Van De Wetering, B. Hofs, Contributions of homogeneous, heterogeneous and biological iron(II) oxidation in aeration and rapid sand filtration (RSF) in field sites, J. Water Supply: Res. Technol.–AQUA 65 (2016) 195–207, https://doi.org/10.2166/aqua.2015.059.
[3] AquaMinerals B.V. Annual Report 2023. Nieuwegein, Netherlands. n.d.
[4] T. Ahmad, K. Ahmad, M. Alam, Sustainable management of water treatment sludge through 3'R' concept, J. Clean. Prod. 124 (2016) 1–13, https://doi.org/10.1016/j.jclepro.2016.02.073.
[5] R. Goedhart, S. Müller, M.C.M. van Loosdrecht, D. van Halem, Vivianite precipitation for iron recovery from anaerobic groundwater, Water Res. 217 (2022) 118345, https://doi.org/10.1016/j.watres.2022.118345.
[6] G.W. Luther, D. Rickard, Chemistry of iron sulfides, Chem. Rev. 107 (2007) 514–562.
[7] I.B. Butler, D. Rickard, Framboidal pyrite formation via the oxidation of iron (II) monosulfide by hydrogen sulphide, Geochim. Cosmochim. Acta 64 (2000) 2665–2672, https://doi.org/10.1016/S0016-7037(00)00387-2.
[8] D. Rickard, Sulfidic Sediments and Sedimentary Rocks 1st ed., vol. 65, Elsevier, Amsterdam, 2012.
[9] D. Rickard, A. Griffith, A. Oldroyd, I.B. Butler, E. Lopez-Capel, D.A.C. Manning, D. C. Apperley, The composition of nanoparticulate mackinawite, tetragonal iron(II) monosulfide, Chem. Geol. 235 (2006) 286–298, https://doi.org/10.1016/j.chemgeo.2006.07.004.
[10] N.G. Harmandas, E. Navarro Fernandez, P.G. Koutsoukos, Crystal growth of pyrite in aqueous solutions. inhibition by organophosphorus compounds, Langmuir 14 (1998) 1250–1255, https://doi.org/10.1021/la970354c.
[11] Y.K. Alduailej, K.S. Sorbie, Iron sulfide scale formation: a new anaerobic setup and new insights, in: Day 2 Thu June 25 2020, SPE, Virtual, 2020, https://doi.org/10.2118/200660-MS (p. D022S009R005).
[12] H. Xian, J. Zhu, X. Liang, H. He, Morphology controllable syntheses of micro- and nano-iron pyrite mono- and poly-crystals: a review, RSC Adv. 6 (2016) 31988–31999, https://doi.org/10.1039/C6RA04874A.
[13] H. Jusoh, N. Sapari, R.Z.R. Azie, Removal of iron from groundwater by sulfide precipitation, World Acad. Sci. Eng. Technol. Int. J. Environ. Chem. Ecol. Geol. Geophys. Eng. (2011) 652–658.
[14] I. Butler, D. Rickard, An anoxic chemostat for controlled sulphide mineral synthesis, Appl. Earth Sci. 112 (2003) 181–182, https://doi.org/10.1179/037174503225002036.
[15] D. Rickard, S. Grimes, I. Butler, A. Oldroyd, K.L. Davies, Botanical constraints on pyrite formation, Chem. Geol. 236 (2007) 228–246, https://doi.org/10.1016/j.chemgeo.2006.09.011.
[16] D.L. Parkhurst, C.A.J. Appelo, Description of Input and Examples for PHREEQC Version 3: A Computer Program for Speciation, Batch-reaction, One-dimensional Transport, and Inverse Geochemical Calculations, U.S. Geological Survey, Reston, VA, 2013, https://doi.org/10.3133/tm6A43.
[17] B. Kiilerich, A.H. Nielsen, J. Vollertsen, Kinetics of sulfide precipitation with ferrous and ferric iron in wastewater, Water Sci. Technol. 78 (2018) 1071–1081, https://doi.org/10.2166/wst.2018.382.
[18] L.L. Bridgewater, R.B. Baird, A.D. Eaton, E.W. Rice, American Public Health Association, American Water Works Association, Water Environment Federation (Eds.), Standard Methods for the Examination of Water and Wastewater, 23rd edition, American Public Health Association, Washington, DC, 2017.
[19] R.J. Cassella, L.G. de Oliveira, R.E. Santelli, On line dissolution of ZnS for sulfide determination in stabilized water samples with zinc acetate, using spectrophotometry by methylene blue method, Spectrosc. Lett. 32 (1999) 469–484, https://doi.org/10.1080/00387019909349999.
[20] M. Monachon, M. Albelda-Berenguer, T. Lombardo, E. Cornet, F. Moll-Dau, J. Schramm, K. Schmidt-Ott, E. Joseph, Evaluation of bio-based extraction methods by spectroscopic methods, Minerals 10 (2020) 203, https://doi.org/10.3390/min10020203.
[21] M. Wolthers, S.J.V.D. Gaast, D. Rickard, The structure of disordered mackinawite, Am. Mineral. 88 (2003) 2007–2015, https://doi.org/10.2138/am-2003-11-1245.
[22] D. Rickard, Kinetics of FeS precipitation: part 1. Competing reaction mechanisms, Geochim. Cosmochim. Acta 59 (1995) 4367–4379, https://doi.org/10.1016/0016-7037(95)00251-T.
[23] R. Bolney, M. Grosch, M. Winkler, J. van Slageren, W. Weigand, C. Robl, Mackinawite formation from elemental iron and sulfur, RSC Adv. 11 (2021) 32464–32475, https://doi.org/10.1039/D1RA03705F.
[24] J. He, C.J. Miller, R. Collins, D. Wang, T.D. Waite, Production of a surface-localized oxidant during oxygenation of mackinawite (FeS), Environ. Sci. Technol. 54 (2020) 1167–1176, https://doi.org/10.1021/acs.est.9b03975.
[25] C. Schröder, M. Wan, I.B. Butler, A. Tait, S. Peiffer, C.A. McCammon, Identification of mackinawite and constraints on its electronic configuration using Mössbauer spectroscopy, Minerals 10 (2020) 1090, https://doi.org/10.3390/min10121090.
[26] J.W. Morse, T. Arakaki, Adsorption and coprecipitation of divalent metals with mackinawite (FeS), Geochim. Cosmochim. Acta 57 (1993) 3635–3640, https://doi.org/10.1016/0016-7037(93)90145-M.
[27] I.B. Butler, C. Archer, D. Vance, A. Oldroyd, D. Rickard, Fe isotope fractionation on FeS formation in ambient aqueous solution, Earth Planet. Sci. Lett. 236 (2005) 430–442, https://doi.org/10.1016/j.epsl.2005.05.022.
[28] I.B. Butler, M.E. Böttcher, D. Rickard, A. Oldroyd, Sulfur isotope partitioning during experimental formation of pyrite via the polysulfide and hydrogen sulfide pathways: implications for the interpretation of sedimentary and hydrothermal pyrite isotope records, Earth Planet. Sci. Lett. 228 (2004) 495–509, https://doi.org/10.1016/j.epsl.2004.10.005.
[29] D.T. Rickard, Kinetics and mechanism of pyrite formation at low temperatures, Am. J. Sci. 275 (1975) 636–652, https://doi.org/10.2475/ajs.275.6.636.
[30] G.W. Luther, Pyrite synthesis via polysulfide compounds, Geochim. Cosmochim. Acta 55 (1991) 2839–2849, https://doi.org/10.1016/0016-7037(91)90449-F.
[31] D. Rickard, G.W. Luther, Kinetics of pyrite formation by the H2S oxidation of iron (II) monosulfide in aqueous solutions between 25 and 125°C: the mechanism, Geochim. Cosmochim. Acta 61 (1997) 135–147, https://doi.org/10.1016/S0016-7037(96)00322-5.
[32] D. Rickard, Kinetics of pyrite formation by the H2S oxidation of iron (II) monosulfide in aqueous solutions between 25 and 125°C: the rate equation, Geochim. Cosmochim. Acta 61 (1997) 115–134, https://doi.org/10.1016/S0016-7037(96)00321-3.
[33] A. Kamyshny, A. Goifman, J. Gun, D. Rizkov, O. Lev, Equilibrium distribution of polysulfide ions in aqueous solutions at 25 °C: a new approach for the study of polysulfides' equilibria, Environ. Sci. Technol. 38 (2004) 6633–6644, https://doi.org/10.1021/es049514e.
[34] T. Siu, C.Q. Jia, Kinetic and mechanistic study of reaction between sulfide and sulfite in aqueous solution, Ind. Eng. Chem. Res. 38 (1999) 3812–3816, https://doi.org/10.1021/ie990254x.
[35] J. Bebié, M.A.A. Schoonen, Pyrite surface interaction with selected organic aqueous species under anoxic conditions, Geochem. Trans. 1 (2000) 47, https://doi.org/10.1186/1467-4866-1-47.
[36] B.A. Bilal, H. Tributsch, Thermo-electrochemical reduction of sulfate to sulfide using a graphite cathode, J. Appl. Electrochem. 28 (1998) 1073–1081, https://doi.org/10.1023/A:1003455219932.
[37] W. Su, L. Zhang, Y. Tao, G. Zhan, D. Li, D. Li, Sulfate reduction with electrons directly derived from electrodes in bioelectrochemical systems, Electrochem. Commun. 22 (2012) 37–40, https://doi.org/10.1016/j.elecom.2012.04.030.
[38] I. Mendizabal, Public supply well fields as a valuable groundwater quality monitoring network, Available:, Vrije Universiteit Amsterdam, 2011. https://research.vu.nl/en/publications/public-supply-well-fields-as-a-valuable-groundwater-quality-monit.
[39] M.L. McFarland, T.L. Provin, Hydrogen sulfide in drinking water - causes and treatment alternatives, Available:, Texas A&M Agrilife Extension, 2021. https://bee.agrilife.org/files/2019/01/Hydrogen-Sulfide-in-Drinking-Water-causes-and-treatment-alternatives.pdf.
[40] S. Peiffer, W. Gade, Reactivity of ferric oxides toward H2S at low pH, Environ. Sci. Technol. 41 (2007) 3159–3164, https://doi.org/10.1021/es062228d.
[41] R.-M. Couture, J. Rose, N. Kumar, K. Mitchell, D. Wallschläger, P. Van Cappellen, Sorption of arsenite, arsenate, and thioarsenates to iron oxides and iron sulfides: a kinetic and spectroscopic investigation, Environ. Sci. Technol. 47 (2013) 5652–5659, https://doi.org/10.1021/es3049724.
[42] M. Wolthers, L. Charlet, C.H. van Der Weijden, P.R. van der Linde, D. Rickard, Arsenic mobility in the ambient sulfidic environment: sorption of arsenic(V) and arsenic(III) onto disordered mackinawite, Geochim. Cosmochim. Acta 69 (2005) 3483–3492, https://doi.org/10.1016/j.gca.2005.03.003.
[43] X. Zhang, H. Fan, J. Yuan, J. Tian, Y. Wang, C. Lu, H. Han, W. Sun, The application and mechanism of iron sulfides in arsenic removal from water and wastewater: a

critical review, J. Environ. Chem. Eng. 10 (2022) 108856, https://doi.org/10.1016/j.jece.2022.108856.
[44] R. Li, J. Niu, X. Zhan, B. Liu, Simultaneous removal of nitrogen and phosphorus from wastewater by means of FeS-based autotrophic denitrification, Water Sci. Technol. 67 (2013) 2761–2767, https://doi.org/10.2166/wst.2013.200.
[45] Y. Yang, T. Chen, M. Sumona, B.S. Gupta, Y. Sun, Z. Hu, X. Zhan, Utilization of iron sulfides for wastewater treatment: a critical review, Rev. Environ. Sci. Biotechnol. 16 (2017) 289–308, https://doi.org/10.1007/s11157-017-9432-3.
[46] J. Pan, L. Liu, H. Pan, L. Yang, M. Su, C. Wei, A feasibility study of metal sulfide (FeS and MnS) on simultaneous denitrification and chromate reduction, J. Hazard. Mater. 424 (2022) 127491, https://doi.org/10.1016/j.jhazmat.2021.127491.
[47] S. Sühnholz, A. Gawel, F.-D. Kopinke, K. Mackenzie, Evidence of heterogeneous degradation of PFOA by activated persulfate – FeS as adsorber and activator, Chem. Eng. J. 423 (2021) 130102, https://doi.org/10.1016/j.cej.2021.130102.
[48] S.-R. Yang, C.-S. He, Z.-H. Xie, L.-L. Li, Z.-K. Xiong, H. Zhang, P. Zhou, F. Jiang, Y. Mu, B. Lai, Efficient activation of PAA by FeS for fast removal of pharmaceuticals: the dual role of sulfur species in regulating the reactive oxidized species, Water Res. 217 (2022) 118402, https://doi.org/10.1016/j.watres.2022.118402.